Flow visualisation experiments for turbine film cooling

C. A. Coat and G. D. Lock
Department of Mechanical Engineering
University of Bath, UK

ABSTRACT

Flow visualisation experiments related to turbine film cooling have been conducted. These investigated the fluid mechanics of coolant ejection using a large-scale, flat-plate model at engine-representative Reynolds numbers in a low-speed tunnel with ambient-temperature mainstream flow. The coolant trajectories were captured using a fine nylon mesh covered with thermochromic liquid crystals, allowing measurement of gas temperature contours in planes perpendicular to the flow. Three injection geometries were assessed: cylindrical holes with stream-wise injection, cylindrical holes with cross-stream injection, and fan-shaped holes. The data demonstrated that the cylindrical holes produced discrete jets, which lifted off the surface at high coolant-to-mainstream momentum flux ratios; these jets were characterised by the kidney-shaped stream-tubes expected for injection into cross-flow. The jets injected with cross-stream momentum exhibited a more obvious kidney-shaped cross-section, which rotated with distance downstream of injection. The jets from the fan-shaped holes were attached to the surface even at high momentum flux ratios, were more diffuse, and exhibited two cores of high temperature. The trajectory visualisation data were used to interpret the adiabatic cooling effectiveness measured at the surface.

NOMENCLATURE

d	hole diameter
I_{actual}	actual momentum flux ratio
I_{ideal}	ideal momentum flux ratio
p	hole pitch
P	pressure
$\mathrm{Re_d}$	Reynolds number based on hole diameter and mainstream flow conditions,
T	temperature
v	flow velocity
x, y, z	cartesian co-ordinates

Greek symbols

η_{aw}	adiabatic cooling effectiveness
η_{gas}	gas effectivensess
μ	dynamic viscosity
ρ	density

Subscripts

aw	adiabatic wall
c	coolant
m	gas, mainstream
mesh	measured on the mesh
o	total, stagnation conditions

1.0 INTRODUCTION

The specific work of gas turbines increases with higher gas temperature and typical modern engines experience turbine entry temperatures (TET) of up to 1,800K. At these elevated temperatures, the turbine components (discs, nozzle guide vanes and rotor blades) require cooling for safe operation and acceptable lifetime. Increasing

Paper No. 2871. Manuscript received 21 January 2002, revised version received 9 December 2003, accepted 4 March 2004.

https://doi.org/10.1017/S000192400000021X Published online by Cambridge University Press

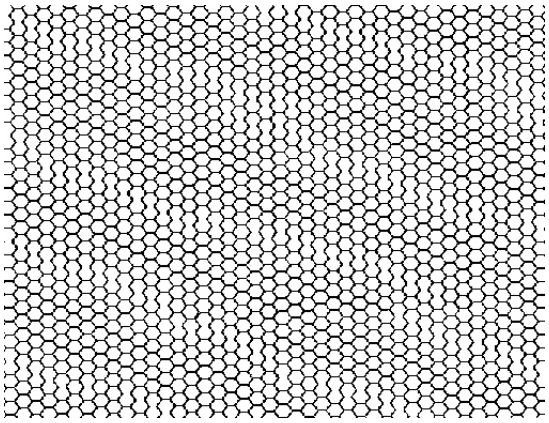


Figure 1. Nylon mesh.

the mass flow rate of coolant allows an increase in the TET, which is the main objective of using cooling flow. However, effective turbine cooling incurs a thermodynamic cost: firstly the compressed air is diverted from the main flow and not used in combustion; secondly there are coolant pressure losses in the feed, delivery and blade passages; and, thirdly, the viscous mixing of coolant with the mainstream after ejection will reduce the aerodynamic efficiency of the turbine. Typically, the TET can be raised by 100K for each additional 1% of coolant flow but with a resultant loss of 1% in turbine efficiency[1]. The engine designer has the task of creating a coolant system that optimises the specific fuel consumption using a compromise between increased TET and this reduced turbine efficiency.

Designers can obtain some information using turbine-based rigs running close to the engine-operating environment. However, deeper insight can be gained from fundamental research that measures, computes and explains the flow and heat transfer in generic, fully-instrumented rigs operating under more benign conditions. Computational codes, validated on these detailed measurements, can then be used to conduct calculations extrapolated to engine conditions.

An understanding of the interaction between the coolant-jet and mainstream flows is crucial to the accuracy of computational fluid dynamic methods and hence to the design of advanced film-cooling geometries. Such an understanding can be achieved with measurements of temperature and velocity in fluid-dynamic conditions carefully generated to simulate the engine. Bird *et al*[2], Ahn *et al*[3] and Honami *et al*[4] have presented temperature and velocity contours for injected coolant using traversing hot-wire anemometry and thermocouple probes. Studies by Mee *et al*[5] and, more recently, Sargison *et al*[6] introduced a new technique: a nylon mesh coated with thermochromic liquid crystals (TLC, see Ireland and Jones[7]) stretched across the flow to capture temperature contours. This technique is inherently obtrusive but has the advantage that qualitative flow visualisation information and quantitative temperature contours over a wide area can be obtained in a single experiment.

The current work has tested three turbine-cooling geometries under engine-representative conditions using the nylon-mesh technique. Both qualitative flow-visualisation information as well as quantitative gas-effectiveness measurements are presented. The cooling effectiveness measured on an adiabatic wall downstream of injection has been correlated with data obtained using the mesh. The flow visualisation experiments presented in this paper were developed in order to increase the understanding of the physical mechanisms governing film-cooling performance.

2.0 EXPERIMENTAL TECHNIQUE

The experiments were conducted in the University of Bath low-speed wind tunnel, which produces mainstream velocities of 25ms^{-1} with less than 1% freestream turbulence. The mainstream total pressure and temperature were at standard atmospheric conditions, and the Reynolds number (based on coolant hole diameter) was typically 36,000. The coolant was a secondary airflow supplied from a pressurised source and heated to an elevated level between 30-60°C (depending upon the experimental requirements) *en route* to an insulated plenum chamber where the pressure and temperature were monitored. The coolant mass flow rate was measured using a BS 1042 orifice plate. The coolant-to-mainstream momentum flux ratio, I_{actual}, could be varied between 3 and 12, which is typical of that expected at the leading-edge of a turbine blade or vane.

2.1 Description of the mesh

The mesh, shown schematically in Fig. 1, was identical to the one used by Sargison *et al*[6]. It was made of fine nylon fibres, less than 0·2mm in diameter, arranged in hexagonal cells of 2mm width. This net was stretched onto a frame and placed across the flow at different positions downstream of coolant injection. A digital camera and light were mounted in the tunnel well downstream of the mesh to record the TLC colour changes at different coolant temperatures.

The mesh was sprayed with narrow-band TLC, calibrated using a K-type thermocouple. The TLC was supplied by Hallcrest and two types were used: narrow band crystals (NBC) and wide band crystals (WBC). Two NBCs were used and coded as R30C1W and R40C1W, indicating that these crystals were active (display colour from red to green to blue) over 1°C wide and nominally at 30 and 40°C respectively. These TLC were calibrated with the mid green colour at 30·5 and 40·2°C respectively. A single R25C8W WBC was used, which was calibrated (in situ) to be active between 24 and 35°C.

The NBC crystals were calibrated on the mesh with a K-type thermocouple. The mesh was mounted into a calibration pipe with heated flow and the hue an intensity recorded over a range of temperatures. The NBC crystal is relatively insensitive to viewing and lighting angles and so only these, rather than the WBC, were used for experiments conducted using the mesh. The measurements of temperature by thermocouples in the free-stream and threaded into the mesh in the jet-pipe calibration described above were equal within experimental uncertainty. The measurement uncertainty is estimated at ±0·2°C.

The mesh fibres were fine and created a net of low aerodynamic resistance: Wang *et al*[8] measured an 8%-loss in dynamic head for a similar mesh. The TLC provide a measurement of the nylon-mesh temperature which is assumed to be that of the gas flowing through it. The thermal conductivity of the fibres and the temperature gradients within it are low, and so the conduction along the net was negligible compared with the heat convected from the flow.

The WBC was used on the rhoacell, adiabatic surface. The WBC was calibrated *in situ* (i.e. in the wind tunnel) under identical lighting conditions and viewing angles as the experiment. An isothermal copper plate, coated in WBC, was electrically heated and the surface temperature measured using an embedded thermocouple. This calibration method is described by Syson *et al*[9] and typically provides a measurement accuracy of ±0·2°C.

2.2 Experimental apparatus

Three film-cooling hole configurations were tested in the current work: (*i*) cylindrical holes with stream-wise injection, (*ii*) cylindrical holes with cross-stream injection, and (*iii*) fan-shaped holes with forward expansion as seen in Fig. 2. The diameter of the cylindrical holes was 23mm providing a mainstream flow Reynolds number (based on this diameter) of 36,000, which is typical of that expected in the engine. The length-to-diameter (*L*/*d*) and pitch-to-diameter

https://doi.org/10.1017/S000192400000021X Published online by Cambridge University Press

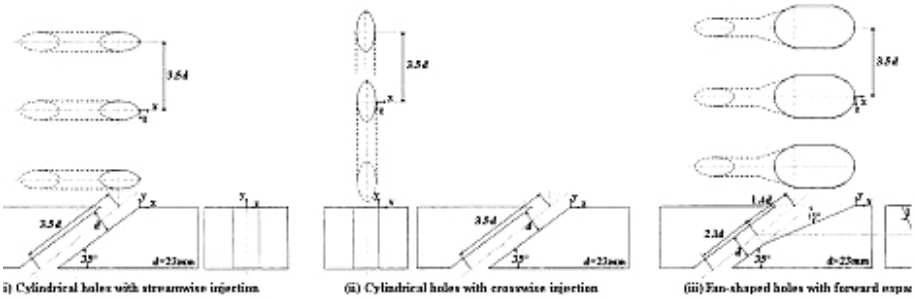


Figure 2. Film-cooling hole geometries.

(p/d) ratios were 3·5 for each hole geometry. The fan-shaped hole was expanded at an angle of 15 degrees in both forward and sideways directions, which results in an elliptical shape at the surface. Each configuration was inclined at the same angle of 35 degrees.

The holes were machined into interchangeable plates. These plates, the plenum chamber, and the surface in the vicinity and downstream of the cooling holes were made from Rohacell, a low conductivity foam. The internal passages of the holes, the plenum chamber and the external surface exposed to the mainstream flow and coolant were considered adiabatic.

2.3 Measurement technique

Two types of experiments were conducted. The first measured contours of film-cooling effectiveness, η_{aw}, on the adiabatic surface downstream of injection. The surface was sprayed with matt-black paint and a wide-band TLC (calibrated *in situ* using a thermocouple and active over a range 25-45°C). During experiment the TLC revealed the local T_{aw} for a given plenum coolant total temperature, T_c, and constant mainstream air temperature, T_m:

$$\eta_{aw} = \frac{T_{aw} - T_m}{T_c - T_m} \quad \ldots (1)$$

It was assumed that the effectiveness was governed by the fluid dynamics only and not influenced by the level of the temperatures (which varied over a modest range $20 < T_c < 60$°C), and this was verified by conducting experiments at constant momentum flux ratio but over a range of coolant temperatures.

The second type of experiments provided temperature measurements on the mesh (located at various positions downstream of injection) using narrow-band crystals, active over a 1°C range. Narrow-band TLC were used as the wide-band variety were difficult to observe and calibrate accurately on the mesh. In addition to providing information about the trajectory, size and structure of the film cooling jets, these experiments produced contours of gas effectiveness off the surface. The gas effectiveness, η_{gas}, is defined similarly to the wall adiabatic effectiveness, with the temperature of the mesh, T_{mesh}, replacing T_{aw}:

$$\eta_{gas} = \frac{T_{mesh} - T_m}{T_c - T_m} \quad \ldots (2)$$

A photograph of the TLC active on the mesh for the case of cross-stream injection at high momentum flux is shown in Fig. 3. Steady-state digital photographs of the crystals (both on the surface and then on the mesh) were recorded for the three film cooling geometries at three different momentum flux ratios. These digital images were subsequently analysed with a MATLAB program to obtain the hue (and hence temperature from calibration) at each pixel in view of the camera.

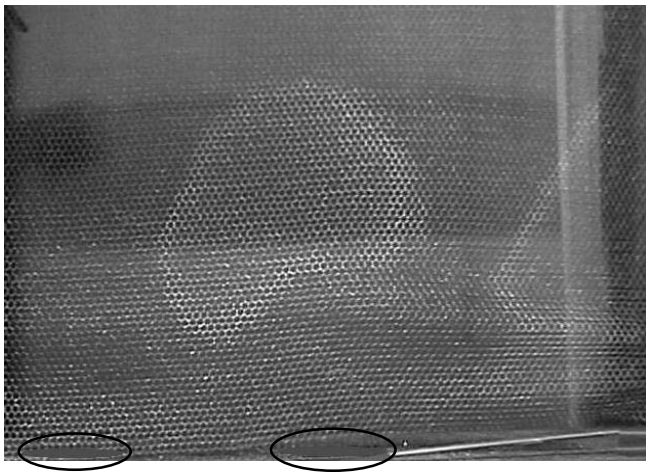


Figure 3. Active TLC on the mesh for cylindrical holes with cross-stream injection at $I_{ideal} = 11$ and $x = 1d$; the holes are circled at the foot of the mesh.

Thermocouples and Pitot probes positioned in the plenum chamber and in the mainstream measured T_c, P_{oc}, T_m, P_m and P_{om}. The velocities were low enough to assume total and static temperatures were essentially equal. These measurements provided a measurement of the ideal coolant-to-mainstream momentum flux ratio:

$$I_{ideal} = \frac{P_{oc} - P_m}{P_{om} - P_m} \quad \ldots (3)$$

The measurement uncertainties in T_c, T_m are estimated at ±0·1°C. The uncertainties for T_{mesh} and T_{aw}, are estimated as ±0·2°C. This creates the estimated uncertainties as follows:
Effectiveness on the surface: ±3%
Effectiveness on the mesh: ±5%
Momentum flux ratio: ±3%

https://doi.org/10.1017/S000192400000021X Published online by Cambridge University Press

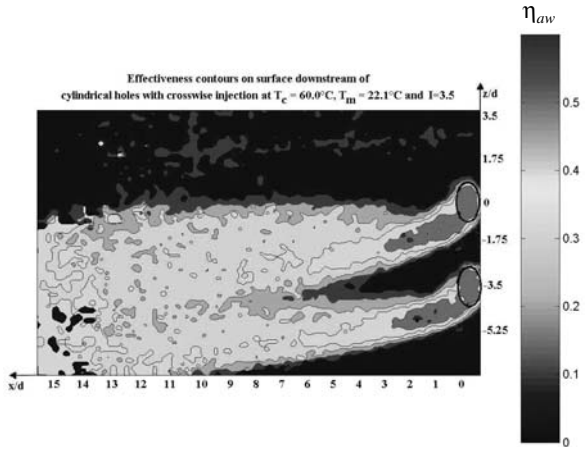


Figure 4. Effectiveness contours on the surface downstream of the injection for cylindrical holes with cross-stream injection and I_{ideal} = 3·5.

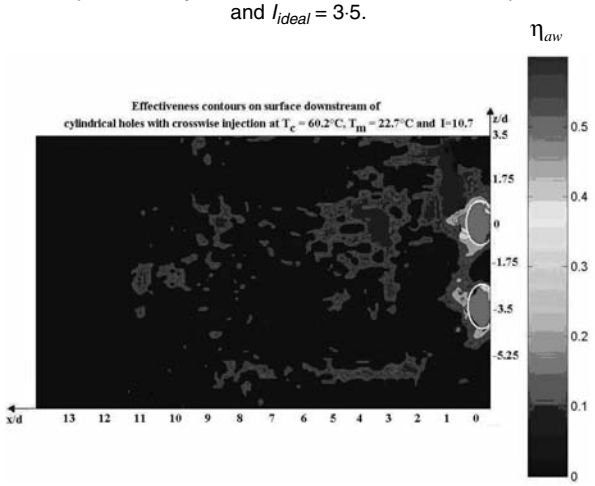


Figure 5. Effectiveness contours on the surface downstream of the injection for cylindrical holes with cross-stream injection and I_{ideal} = 11.

3.0 EXPERIMENTAL RESULTS

3.1 Cylindrical holes with cross-stream injection — adiabatic surface

Figures 4 and 5 illustrate contour maps of adiabatic cooling effectiveness on the surface for the case of cylindrical holes injecting coolant in the cross-stream direction at momentum flux ratios of 3·5 and 11 respectively. Figure 4 reveals high cooling effectiveness immediately downstream of injection, with the cooling 'footprint' influenced by the cross-stream momentum of the coolant. Two discrete footprints are visible, which merge at approximately seven hole-diameters downstream of injection, where the flow from the two holes has mixed to a single wake. Between $0 < x/d < 7$, there is a region of zero cooling effectiveness between the holes.

Figure 5 shows that at the higher momentum flux the adiabatic cooling effectiveness at the wall is essentially zero downstream of injection, despite a larger mass flux of coolant. Here the coolant has lifted off the surface, as revealed by the corresponding measurements obtained with the mesh (discussed in the next section).

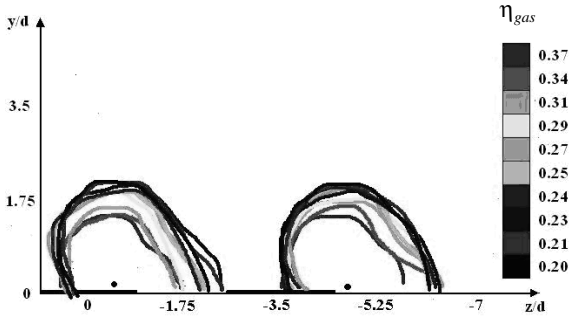


Figure 6. Gas effectiveness contours — cylindrical holes with cross-stream injection at I_{ideal} = 3·5 and $x = 1_d$.

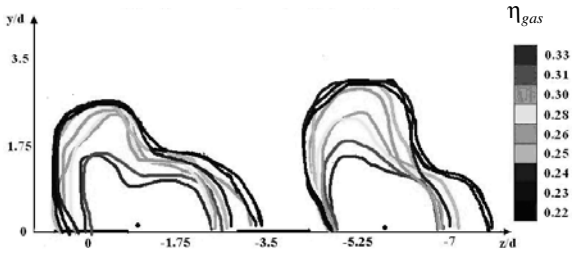


Figure 7. Gas effectiveness contours — cylindrical holes with cross-stream injection at I_{ideal} = 3·5 and $x = 3_d$.

3.2 Cylindrical holes with cross-stream injection — gas effectiveness measurements

Figures 6 and 7 (viewed upstream) show contours of gas effectiveness (essentially isotherms), obtained using the mesh, for the case of cross-stream injection at a momentum flux ratio of 3·5. The measurements are shown at 1 and 3 diameters downstream and correspond to the surface adiabatic measurements shown in Fig. 4. The hole positions (z/d = 0 and –3·5) are also marked in these figures.

These figures show that the jets remain attached to the wall, explaining the good cooling performance on the surface. The emerging coolant features a core of high gas effectiveness with a strong gradient in temperature at the edges of the jet. The cross-stream momentum of the injected coolant has shifted the core to the right (negative z direction) and created an asymmetric temperature field. The core is shifted further to the right with increasing downstream position. The mainstream, with low temperature, has penetrated into the left side of the jet, whereas no penetration of the low-temperature fluid occurs on the right side. The two coolant trajectories are still separate at x/d = 3, as expected from the non-cooled region between the holes observed in Fig. 4. At the further downstream position the coolant jet is thicker and more diffuse as the coolant spreads and mixes with the mainstream flow. The peak temperature in the core is seen to decrease with downstream distance.

Figures 8-10 show contours of gas effectiveness for the case of cross-stream injection at a momentum flux ratio of 11. The measurements are shown at 1, 3 and 10 diameters downstream and correspond to the adiabatic surface measurements shown in Fig. 5. Only the coolant trajectory for the hole situated at z/d = 0 is shown. These figures illustrate clearly that the coolant jets have lifted off the surface, penetrating into the mainstream, and explain the poor adiabatic effectiveness on the surface. Again the cross-stream momentum has shifted the coolant trajectory to the right (negative z) but the larger momentum flux has pushed the core further across the mainstream than the cases shown in Figs 7 and 8. The coolant jets

https://doi.org/10.1017/S000192400000021X Published online by Cambridge University Press

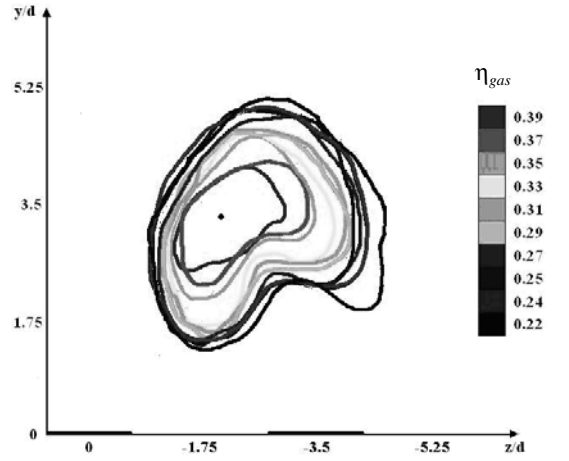


Figure 8. Gas effectiveness contours — cylindrical holes with cross-stream injection at $I_{ideal} = 11$ and $x = 1_d$.

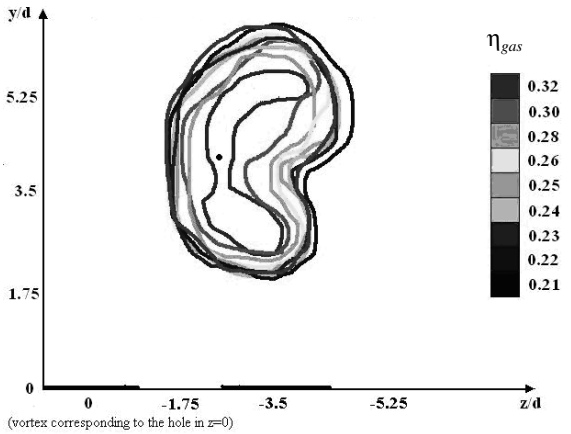


Figure 9. Gas effectiveness contours — cylindrical holes with cross-stream injection at $I_{ideal} = 11$ and $x = 3_d$.

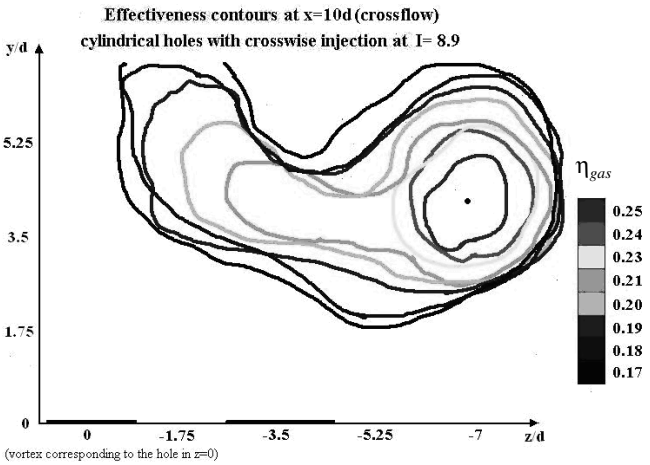


Figure 10. Gas effectiveness contours — cylindrical holes with cross-stream injection at $I_{ideal} = 11$ and $x = 10_d$.

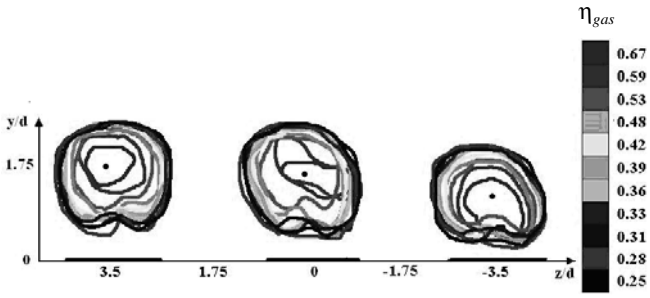


Figure 11. Gas effectiveness contours — cylindrical holes with cross-stream injection at $I_{ideal} = 11$ and $x = 1_d$.

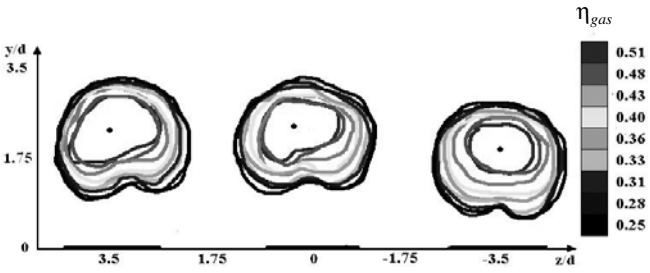


Figure 12. Gas effectiveness contours — cylindrical holes with cross-stream injection at $I_{ideal} = 11$ and $x = 3_d$.

are highly asymmetric, featuring a kidney-shaped cross-section (discussed in Section 3.3). The jet is observed to rotate anti-clockwise as it moves downstream, with the jet core temperature decreasing with distance downstream.

There were some differences between the adiabatic effectiveness at the wall and the gas effectiveness obtained by the mesh near the wall. However, this was to be expected as there was no frame on the mesh near the wall and thus a limit on how close to the wall measurements using the mesh could be achieved.

3.3 Cylindrical holes with stream-wise injection — gas effectiveness

Figures 11 and 12 show gas effectiveness contours at x/d =1 and 3 for the case of injection in the stream-wise direction at a coolant-to-mainstream momentum flux ratio of 11. The three coolant holes are located at z/d = 0 and ±3·5. The coolant jets are separate and have completely penetrated into the mainstream. Though the trajectory has no cross-stream (z-direction) motion, the core of the jet is observed to have upward (y-direction) momentum.

The jets exhibit the kidney-shaped cross-section predicted by Haven and Kurosaka[10] and shown schematically in Fig. 13. The coolant jet follows a curved trajectory and a secondary flow within the core creates a pair of kidney vortices, which direct the sides of the jet down towards the surface and the core of the jet upwards. Mainstream flow is entrained along the sides of the jet towards the surface, which is generally detrimental to cooling performance. The net fluid-dynamic effect is a secondary motion which increases lift

https://doi.org/10.1017/S000192400000021X Published online by Cambridge University Press

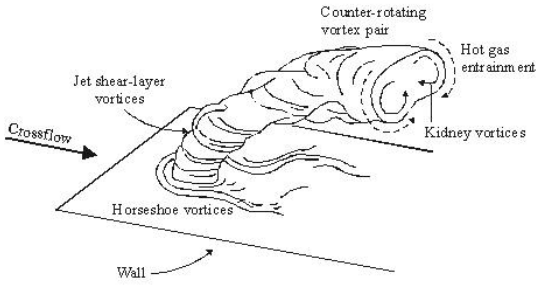


Figure 13. Formation of the kidney-shaped cross section.

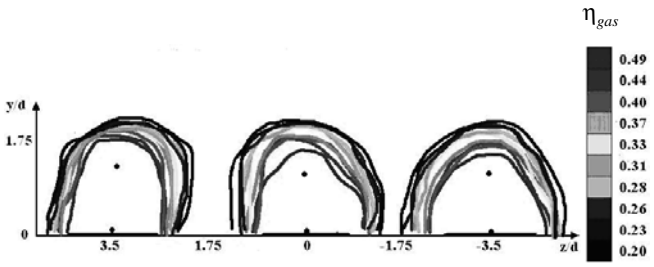


Figure 14. Gas effectiveness contours — fan-shaped holes with stream-wise injection at I_{ideal} = 11 and $x = 1_d$.

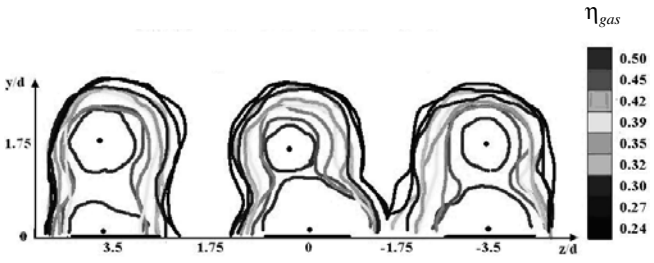


Figure 15. Gas effectiveness contours — fan-shaped holes with stream-wise injection at I_{ideal} = 11 and $x = 3_d$.

off. This is potentially detrimental at lower momentum flux ratios where the coolant would otherwise remain attached to the surface.

The kidney-shaped cross-sections are more clearly visible in Figs 8-10. Here there is a complex fluid-dynamic interaction between the rotating jet and the influence of lift off generated by the vortices. In Fig. 8 the vortices create secondary, vertical (y-direction) motion but as the jet rotates to its position shown in Fig. 9, this motion would be in the horizontal (z) direction; in Fig. 10 the 'lift off' would be directed downwards towards the surface. The core of the coolant jet is observed to remain at approximately the same height above the surface, probably due to this interaction.

3.4 Fan-shaped holes with stream-wise injection

Figures 14 and 15 show gas effectiveness contours at x/d = 1 and 3 for the case of injection from fan-shaped holes with forward expansion at a coolant-to-mainstream momentum-flux ratio of 11. The coolant momentum flux was measured in the cylindrical portion of the hole in order to directly compare with the case of injection from cylindrical holes. The three coolant holes are located at z/d = 0 and ±3·5. The jets are separate but unlike the case for the cylindrical

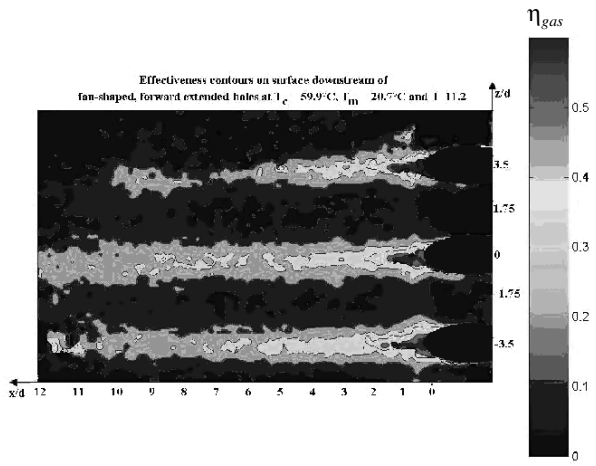


Figure 16. Effectiveness contours on the surface downstream of the injection for fan-shaped holes with cross-stream injection at I_{ideal} = 11.

holes at this momentum-flux ratio, the coolant remains attached to the surface at x/d = 1, probably because the velocity of the coolant emerging from the hole is less due to the larger exit flow area. The current experiments cannot distinguish between the reduced jet velocity at exit and any flow divergence effects associated with the hole geometry as the discharge coefficient of the hole, see Rowbury *et al*[10], was not measured. The consequences of this attached flow is clearly illustrated in Fig. 16, which shows the adiabatic cooling effectiveness on the surface; here the cooling footprints indicate a good cooling performance, despite the large coolant-to-mainstream momentum-flux ratio.

At x/d = 3, the jets are seen to be more diffuse and a double core has developed. Similar results were found over a range of momentum-flux ratios. The presence of two cores might be explained by a divergence of flow within the coolant jet, created by the forward-expansion geometry. The upper core develops as the jet tends to behave like a jet emerging from a cylindrical hole. The lower core might be generated from the sideways expansion at the hole exit, with the low-momentum fluid remaining attached to the surface. The kidney-shaped vortices of the main jet would entrain mainstream flow towards the surface and thus press the second jet against the surface, helping to keep it attached even at high momentum-flux ratio.

The main (upper) core of the jets in Figs 14 and 15 are as closer to the surface than those from the cylindrical jets at the same momentum-flux ratio. This is partially due to the slower velocity of the emerging coolant for the case of forwardly-expanded holes. In addition, the 'lift-off' effect (y-direction movement) of these jets would be expected to be weaker than the corresponding case for cylindrical holes, as explained by Haven and Kurosaka[11], since anti-kidney vortices decrease the lift-off in fan-shaped holes.

4.0 CONCLUSIONS

Flow visualisation experiments have been conducted for three turbine film cooling geometries: cylindrical holes with stream-wise injection, cylindrical holes with cross-stream injection, and fan-shaped holes with forward expansion. The experiments were conducted in a low-speed wind tunnel at engine-representative Reynolds number and coolant-to-mainstream momentum-flux ratios. A low-resistance mesh coated in thermochromic liquid crystals was used to capture the coolant trajectories and measure the gas effectiveness in planes downstream of injection. These results were

https://doi.org/10.1017/S000192400000021X Published online by Cambridge University Press

compared with measurements of film cooling effectiveness on an adiabatic surface. The data helps to provide an understanding of the fluid-dynamics of coolant injection and is also useful in validating CFD codes.

- The coolant trajectories from the cylindrical holes were clearly observed to lift off the surface at high momentum flux ratios; the corresponding cooling effectiveness on the adiabatic wall was measured to be low; the cooling effectiveness on the adiabatic wall was shown to be good for cases where the coolant trajectories remained attached to the surface.
- The coolant jets featured a core of high gas effectiveness with a strong gradient in temperature at the edges of the jet; the jets were shown to be diffuse, with the core temperature decreasing with distance downstream from injection.
- Cross-stream injection featured jets with an asymmetric structure due to the lateral component of momentum of the coolant; the jets were observed to rotate with distance downstream of injection.
- The jets from cylindrical holes exhibited a kidney-shaped cross-section created by a vortex-structure in the flow.
- The coolant jets from fan-shaped holes with a forward-expansion geometry featured two cores of high temperature; the flow from these holes remained attached to the surface even at high coolant-to-mainstream momentum flux ratios, with corresponding good surface cooling effectiveness.

ACKNOWLEDGMENTS

Caroline Coat conducted this research at Bath while a student at the Ecole des Mines, Nancy, France. The authors would like to thank the technician Mr A. Elley. Advice concerning the mesh was generously provided by Dr P. T. Ireland in Oxford.

REFERENCES

1. DENTON, J.D. Loss mechanisms in turbomachines, *ASME J of Turbomachinery*, 1993, **115**, pp 621-656.
2. BURD, S.W., KASZETA, R.W. and SIMON, T.W. Measurements in film cooling flows: Hole *L/D* and turbulence intensity effects, *ASME J of Turbomachinery*, 1998, **120**, pp 791-798.
3. AHN, J., JUNG, I.S. and LEE, J.S. Film cooling from two rows of holes with opposite orientation angles: injection behavior and adiabatic film cooling effectiveness, *Int J of Heat and Fluid Flow*, 2003, **24**, pp 91-99.
4. HONAMI, S., SHIZAWA, T. and UCHIYAMA, A. Behavior of the laterally injected jet in film cooling: measurements of surface temperature and velocity/temperature field within the jet, *ASME J of Turbomachinery*, 1994, **116**, pp 106-112.
5. MEE, D.J., IRELAND, P.T. and BATHER, S. Measurement of the temperature field downstream of simulated leading-edge film-cooling holes, *Experiments in Fluids*, 1999, **27**, pp 273-283.
6. SARGISON, J.E., GUO, S.M., OLDFIELD, M.L.G., LOCK, G.D. and RAWLINSON, A.J. Flow visualisation of a converging slot-hole film-cooling geometry, 2002, ASME Paper GT-2002-30177.
7. IRELAND, P.T. and JONES, T.V. Liquid crystal measurements of heat transfer and surface shear stress. *Meas Sci Technol*, 2000, **11**, pp 969-986.
8. WANG, Z., IRELAND, P.T. and KOHLER, S.T. Gas temperature measurement in internal cooling passages, 1996, ASME Paper 96-GT-534.
9. SYSON, B.J., PILBROW, R.G. and OWEN, J.M. Effect of rotation on temperature response of thermochromic liquid crystal, *Int J of Heat and Fluid Flow*, 1999, **17**, pp 491-499.
10. ROWBURY, D.A., OLDFIELD, M.L.G. and LOCK, G.D. A method of correlating the influence of external crossflow on the discharge coefficient of film cooling holes, *ASME J of Turbomachinery*, 2001, **123**, pp 258-265.
11. HAVEN, B.A. and KUROSAKA, M. Kidney and anti-kidney vortices in crossflow jets. *J Fluid Mech*, 1997, **352**, pp 27-64.

https://doi.org/10.1017/S000192400000021X Published online by Cambridge University Press